Quantitative Depth Profiling of Layered Samples Using Phase-Modulation FT-IR Photoacoustic Spectroscopy

ROGER W. JONES* and JOHN F. McCLELLAND

Ames Laboratory–USDOE, Iowa State University, Ames, Iowa 50011 (R.W.J., J.F.M.); and MTEC Photoacoustics, Inc., Ames, Iowa 50014 (J.F.M.)

In phase-modulation FT-IR spectroscopy, all wavelengths in a spectrum are modulated at the same frequency and in phase. This factor makes the use of photoacoustic phase data for depth profiling samples much easier in phase modulation than in rapid scan. A method to quantitatively measure layer thickness by using the phase of a substrate spectrum peak is demonstrated with a series of samples consisting of thin polymer films on substrates. Additions to the basic method are demonstrated that extend its application to cases where the substrate peak is overlapped by a spectrum peak of the surface film. A linear relationship between phase angle and layer thickness extending to thicknesses greater than twice the thermal diffusion length is demonstrated. Representations of phase modulation data as a family of angle-specific spectra, as magnitude vs. phase curves, and as a power spectrum and phase spectrum pair, each of which is useful for different aspects of depth profiling, are discussed. Calculating these representations from a single pair of orthogonal interferograms is described.

Index Headings: **Phase modulation; Photoacoustic spectroscopy; Depth profiling.**

INTRODUCTION

Depth profiling by using rapid-scan FT-IR photoacoustic spectroscopy has been performed for a number of years.[1–3] Rapid-scan depth profiling relies on the change of peak heights with interferometer scanning speed, which controls the photoacoustic sampling depth. The sampling depth is conventionally identified with the thermal diffusion length, μ, in the sample material:[2–4]

$$\mu = \left(\frac{D}{\pi v \bar{\nu}}\right)^{1/2} \quad (1)$$

where D is the thermal diffusivity of the material, v is the scanning (retardation) velocity of the interferometer, and $\bar{\nu}$ is the infrared wavenumber. Although this approach has proven useful in many cases, it has several shortcomings. The dependence of the thermal diffusion length on $\bar{\nu}$ means that μ varies across a spectrum. The square root dependence of μ on v means that a wide range of scanning speeds is required for depth profiling over a reasonable depth range. Most importantly, photoacoustic sensitivity does not end abruptly at a depth of one diffusion length, but tapers off smoothly, so that depth resolution is diffuse. Lastly, using only peak heights ignores the phase of a photoacoustic signal, which is directly related to the depth at which the infrared absorption occurs.[5] Unfortunately, phase is difficult to extract from rapid-scan data.[6]

The advent of commercial step-scanning FT-IR spectrometers has opened up the possibility of using photoacoustic phase information. In step scanning, the interferogram is taken point by point. The interferometer retardation is fixed while each data point is taken and changes abruptly between points. A second, faster, modulation, independent of the interferometer scanning, can therefore be introduced and used as the signal carrier.[6–8] This second modulation can be induced in the sample itself, as in polymer rheo-optical studies.[6,7] For photoacoustic spectroscopy, it is best to modulate the infrared beam via phase modulation,[6,8] in which an interferometer mirror dithers to oscillate the retardation about the set point of each interferometer step. This approach modulates all wavelengths synchronously, and lock-in demodulation can be used to extract the phase-modulation induced signal. A two-channel lock-in provides access to both magnitude and phase via in-phase and quadrature component interferograms.

The depth-profiling capabilities of phase-modulation FT-IR photoacoustic spectroscopy have been studied by previous authors.[6,8–13] They have shown that spectrum changes with detection phase angle can be used to characterize the sample depth range over which components are distributed, and they have shown that spectra acquired at the proper phase angles can isolate the spectra of individual layers in two-layer samples. Only recently have authors given reports quantitatively relating phase-modulation phase to sample depth.[12,13] Jiang et al.[13] have developed theory for the case of layered samples in which each layer has a unique absorption band; that is, each layer has a wavenumber at which only it absorbs—all other layers are transparent. They relate the difference in phase between peaks arising from different layers to a combination of sample depths, thermal diffusion lengths, and absorption coefficients. Jurdana et al.,[12] in their study of keratin fibers, used phase-modulation photoacoustic spectroscopy to derive quantitative depths for sample layers by a different approach. They observed sudden changes in band position as a function of phase angle, and took these changes to indicate the depths of the layers. We have not observed similar position changes with phase in our work. The purpose of this paper is to more thoroughly explore the application of phase-modulation FT-IR photoacoustic spectroscopy to quantitative depth profiling of discretely layered samples. Our approach is consistent with that of Jiang et al.,[13] but extends to cases where absorptions from two layers overlap. We use samples of known structure to test the quantitative accuracy of the technique. In the process, we examine the various representations of phase-modulation photoacoustic data,

Received 29 September 1995; accepted 6 June 1996.
* Author to whom correspondence should be sent.

0003-7028/96/5010-1258$2.00/0

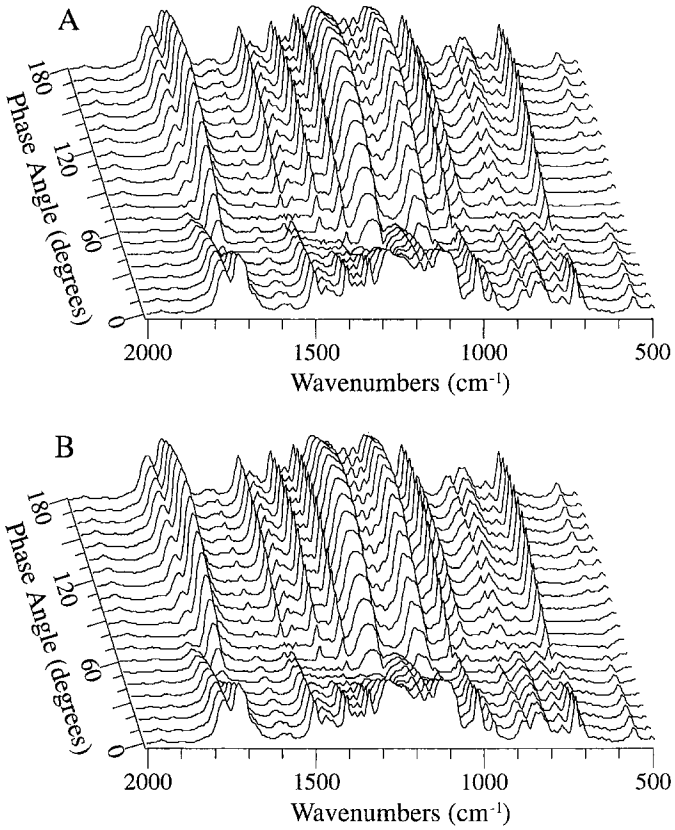

FIG. 1. Angle-specific 400-Hz phase-modulation spectra of a layered sample consisting of a 6-μm PET film on polycarbonate. (**A**) Spectra individually acquired with the demodulator set at each corresponding angle. (**B**) Spectra synthesized from the 0° and 90° interferograms.

their interpretations, and the subject of how to generate them.

EXPERIMENTAL

A Bio-Rad FTS 60A FT-IR spectrometer with a Bio-Rad demodulator and a helium-purged MTEC Model 200 photoacoustic cell was used for all data acquisition. All data were taken with a phase modulation of 400 Hz and 2 laser-fringe (1.266-μm retardation) amplitude with the interferometer step scanning at 25 Hz (632.8-nm retardation shift per step) with 8-cm^{-1} resolution. All interferograms acquired were symmetric, with 16 scans coadded. Except for the spectra in Fig. 1A, all data were derived from orthogonal interferograms taken simultaneously via the two-channel capability of the demodulator. The interferograms were Fourier transformed without phase correction, generating real and imaginary components. The angle-specific spectra are the root mean square (rms) values of these components. It should be noted that the 0° point in the phase angle scale is arbitrary, set by the timing of internal circuits in the spectrometer and demodulator. Although arbitrary, it is exactly repeatable among all spectra taken under the same spectrometer settings, so the phase scale is the same in all data shown.

Each sample consisted of a thin polyethylene terephthalate (PET) layer on a polycarbonate substrate and was made by wetting one surface of a 1.6-mm-thick, 9.5-mm-diameter polycarbonate disk (General Electric Lexan) with 1,2-dichloroethane to soften the plastic, then firmly pressing the disk against a PET film of known thickness (Goodfellow and Chemplex) until the plastic had hardened. Excess film was then trimmed away. When a layered sample was placed in the photoacoustic cell, it was covered with a metal ring to shield the edge of the sample, which may not have been perfectly trimmed, from the infrared beam. A rubber disk containing 65% by weight carbon black was used as the normalization reference.

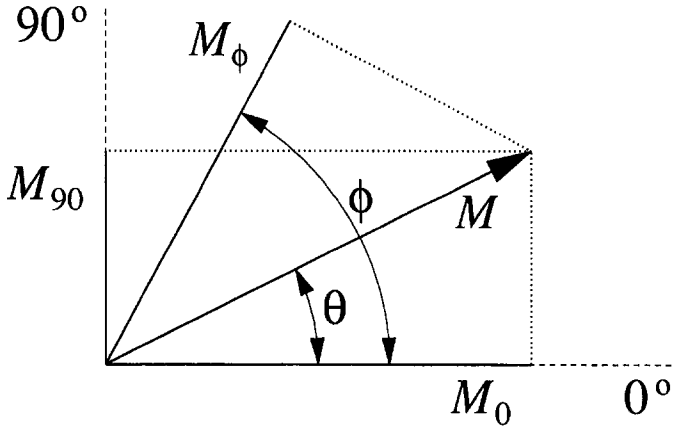

FIG. 2. Relation among a vector of magnitude M and phase θ; its orthogonal components, M_0 and M_{90}; and its projection, M_ϕ, at phase angle ϕ.

RESULTS AND DISCUSSION

Calculating Representations of Data. The most common way of presenting phase-modulation data is as spectra taken at specific phase angles because that is how the data are most often acquired. Recording angle-specific spectra one at a time to generate a complete family, like that shown in Fig. 1A, is a tedious task. Fortunately, this approach is not needed. When phase-sensitive detection is used, the signal at each retardation point along the interferogram or each wavenumber along the spectrum can be considered a vector, which can be represented by its phase and magnitude or in-phase and quadrature components.[6,8–10] The vector in Fig. 2 with a magnitude M and a phase θ is the signal at a single retardation point. Its projections onto the 0° and 90° axes, M_0 and M_{90}, are

$$M_0 = M \cos\theta \quad \text{and} \quad M_{90} = M \sin\theta. \qquad (2)$$

The points of the interferogram at a specific phase angle, ϕ, are then just the projections of these vectors onto the angle, as Fig. 2 shows. Each point, M_ϕ, or the whole interferogram, I_ϕ, at phase ϕ can be related to the vectors and their 0° and 90° components:[8,11]

$$M_\phi = M\cos(\phi - \theta) = M_0\cos\phi + M_{90}\sin\phi \qquad (3)$$

$$I_\phi = I_0\cos\phi + I_{90}\sin\phi \qquad (4)$$

where I_0 and I_{90} are the interferograms at 0° and 90°. The same relations hold for a spectrum and its individual points. It should be noted that for Eq. 4 to hold, I_0 and I_{90} must be synchronized; that is, they must be in step so that data point number n in one interferogram is at the same optical retardation as point n in the other. This synchronization occurs automatically if a two-channel lock-

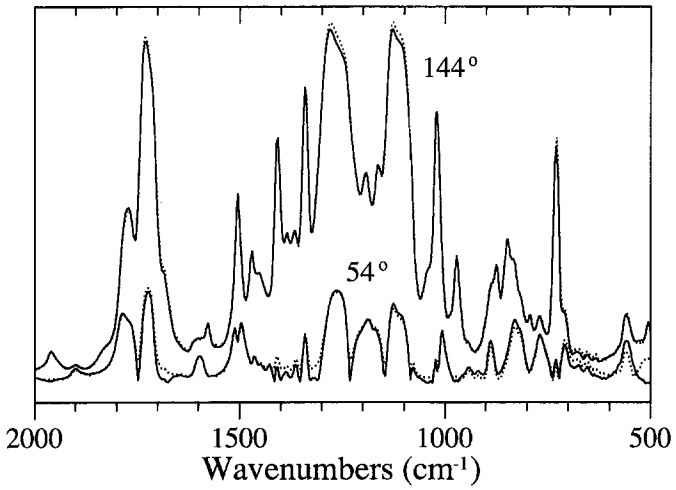

FIG. 3. Two pairs of angle-specific spectra from Fig. 1 at the indicated phase angles comparing (———) individually acquired and (·····) synthesized spectra.

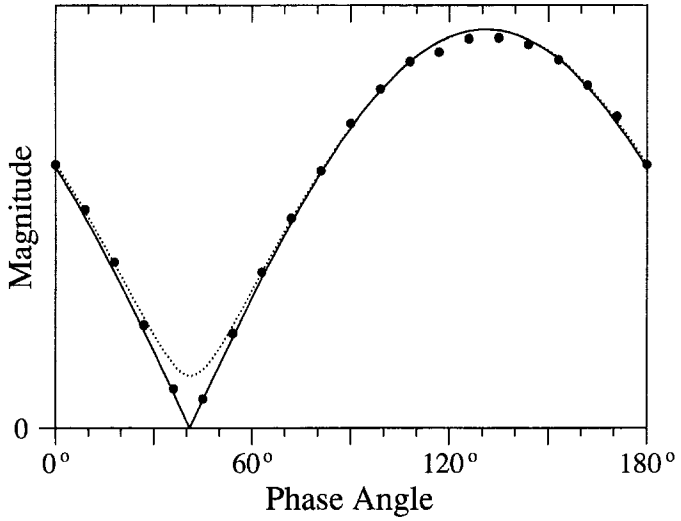

FIG. 4. Phase-angle dependence of the magnitude of the 1730-cm^{-1} PET band from (●) the directly measured spectra in Fig. 1A and (·····) the synthesized spectra in Fig. 1B compared to (———) the function $M|\cos(\phi - 131°)|$.

-in demodulator is used to collect the orthogonal interferograms simultaneously, but may not occur if they are collected one at a time. The interferogram from Eq. 4 can be Fourier transformed in the normal way to generate a single-beam spectrum equivalent to one acquired directly with a lock-in demodulator set to ϕ degrees. As always, the angle-specific spectra must be normalized by using the spectrum of a wide-band absorber reference to remove wavenumber-dependent response variations of the instrument. Angle-specific spectra should not be used for reference, because their use will convolute the phase dependence of the wide-band absorber spectra with that of the sample spectra. Instead, the reference should be a phase-modulation power spectrum, the rms of the in-phase and quadrature spectra (or any two orthogonal spectra).

Figure 1 shows two families of normalized, angle-specific, 400-Hz phase-modulation spectra for a sample consisting of a 6-μm PET film on a thick polycarbonate substrate. The spectra in Fig. 1A were recorded one at a time by stepping the lock-in demodulator through 9° increments. The spectra in Fig. 1B were generated from the 0° and 90° interferograms with Eq. 4. Figure 3 compares two of the directly measured spectra (solid lines) with their synthetic counterparts (dotted lines). The 144° pair is typical of most of the spectra; the directly measured and synthetic spectra are nearly identical. The 54° pair shows the largest mismatch found between the direct and synthetic sets, and they differ the most in weak-signal areas between peaks.

A good representation of the data for visualizing the phase behavior of bands results if a family of angle-specific spectra is rotated 90° so that the magnitudes of individual bands are presented as functions of phase angle. Figure 4 shows such a representation of data drawn from the Fig. 1 spectra for the PET carbonyl band at 1730 cm^{-1}. The circles are the magnitudes of the 1730-cm^{-1} band from the 20 directly measured spectra. The dotted line is the heights of the band from the synthesized spectra. (Data points were taken from more than the 20 spectra shown in Fig. 1B in order to render a smooth curve.) Because an angle-specific interferogram is the geometric projection of the vectors making up the photoacoustic signal, the magnitude at each retardation should be a cosine function of phase angle. When Fourier transformed, this cosine dependence is maintained. Because the transform is to a non-negative spectrum, the dependence takes the form of the absolute value of a cosine. The solid line in Fig. 4 is the function $M|\cos(\phi - \theta)|$, where M and θ are the magnitude and phase (131°) of the observed band maximum in Fig. 4 (the vector in Fig. 2). The band heights from the directly measured data follow the absolute cosine function along the whole curve, but the synthesized-spectra band heights deviate near the minimum. This deviation explains the differences observed between the two 54° spectra in Fig. 3. The two 54° spectra differ most in valleys—wavenumbers were 54° is very near the phase angle of zero magnitude.

As previously discussed, the most concise representation of the data is as a power and phase spectrum pair. The power spectrum is the rms of the 0° and 90° angle-specific spectra, S_0 and S_{90}.[10,11,14] The phase spectrum, S_θ, can also be calculated from S_0 and S_{90}, but because the orthogonal spectra are both non-negative, it cannot be determined from S_0 and S_{90} alone whether the phase falls in the 0° to 90° quadrant or the 90° to 180° quadrant. Some information is lost in transforming from the orthogonal interferogram pair I_0 and I_{90} to the non-negative spectra S_0 and S_{90}. Fortunately, the necessary information can be recovered by using the 45° and 135° spectra, S_{45} and S_{135}, as guides. If that is done, then[10,11,14]

$$S_\theta = \tan^{-1}(S_{90}/S_0) \quad \text{or} \quad S_\theta = \pi - \tan^{-1}(S_{90}/S_0) \quad (5)$$

where the first applies when $S_{45} > S_{135}$ and the latter applies when $S_{45} < S_{135}$. Figure 5 shows the phase and power spectra at 400-Hz phase modulation for the 6-μm PET on polycarbonate sample. Note that the phase varies over a range of about 55°. Theory predicts that the phase of the photoacoustic signal from a homogeneous sample[4,14] or from a homogeneous layer within a sample[13] cannot vary by more than 45°, but the phase for all of a layered sample can vary by more. Theory predicts that

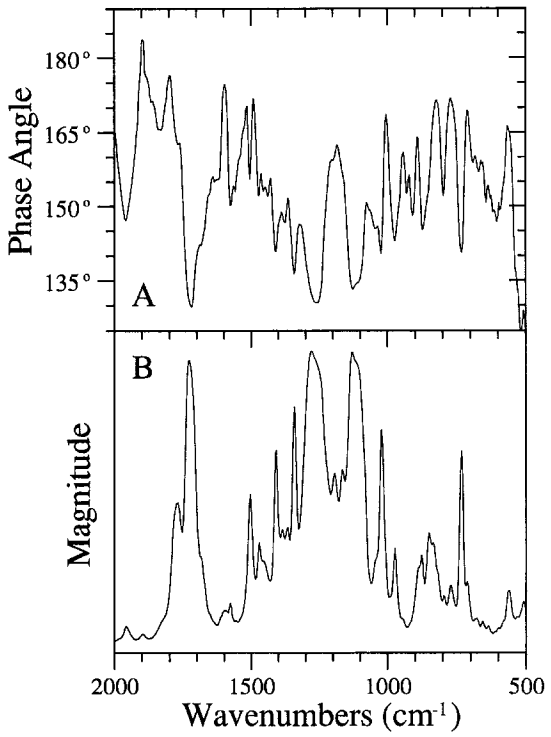

FIG. 5. The 400-Hz phase modulation (**A**) phase and (**B**) power spectra of a layered sample consisting of a 6-μm PET film on polycarbonate.

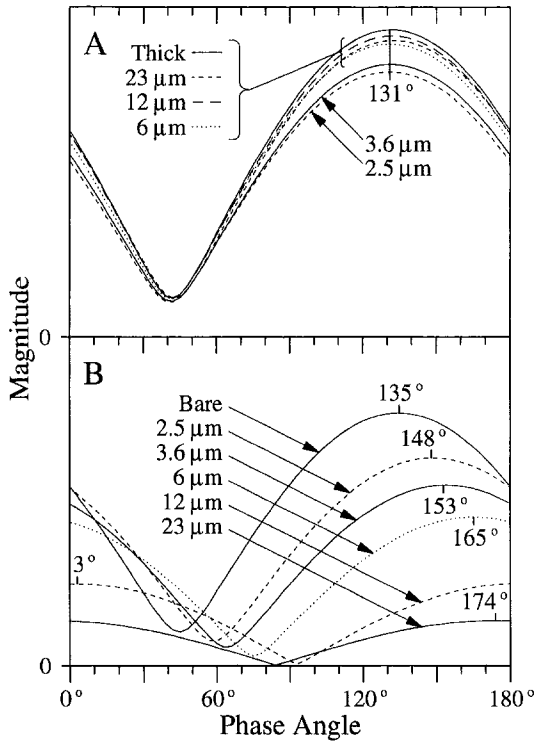

FIG. 6. Phase-angle dependence of the magnitudes of (**A**) the 1730-cm^{-1} PET band and of (**B**) the 1778-cm^{-1} polycarbonate band for a series of layered samples consisting of the indicated thicknesses of PET film on thick polycarbonate substrates. *Thick* in **A** is for a 0.74-mm-thick sheet of PET (without polycarbonate), and *Bare* in **B** is for a bare polycarbonate substrate.

the photoacoustic phase shifts to earlier (i.e., lower) values as the absorption coefficient increases.[4,13,14] Consistent with this prediction, all downward-pointing features in Fig. 5A with phases less than 165° are PET bands. By contrast, infrared absorption by the polycarbonate shifts the phase to higher values (*vide infra*). In general, regions in which the observed phase exceeds 165° are regions where polycarbonate absorptions dominate the photoacoustic signal.

Depth Profiling Uses of the Data Representations. When angle-specific spectra can provide the desired depth profiling information, they are the simplest approach. The spectrum at a specific phase angle eliminates features at the orthogonal angle; thus, choosing a phase angle to eliminate unwanted bands gives better results than choosing one to emphasize desired features. Previous authors[6,8–12] have demonstrated how to use angle-specific spectra in separating out the spectra of individual layers within layered samples, so that subject will not be discussed further here.

The magnitude vs. phase representation of phase modulation data illustrates important aspects of quantitative depth profiling of discretely layered samples. As Adams and Kirkbright[5] have shown, if a sample consists of an absorbing substrate covered by a transparent layer of thickness d, then the thermal wave at the sample surface will lag behind the creation of the wave at the buried layer by a phase $\Delta\theta$:

$$\Delta\theta = \frac{d}{\mu} = d\left(\frac{\pi f}{D}\right)^{1/2} \qquad (7)$$

where f is the modulation frequency, and μ and D are the thermal diffusion length and thermal diffusivity of the transparent overlayer. In phase modulation, μ is not related to scanning speed or wavenumber, as it is in Eq. 1 for rapid scan. Equation 7 means that the phase of a substrate absorption band from the layered sample should lag by $\Delta\theta$ behind the phase of the same band from a bare piece of substrate material, so d can be determined from these two phases, as long as the overlayer can be considered transparent at the wavelength of the substrate absorption.[13]

A series of samples, each consisting of a thin PET film on a thick polycarbonate substrate, was studied to test this relation between photoacoustic phase and film thickness. Figure 6A shows the phase dependence of the 1730-cm^{-1} carbonyl band of PET from these samples, and Fig. 6B shows the same for the 1778-cm^{-1} carbonyl band of polycarbonate. The PET band phase remains fixed at 131° (±2°) for all the samples, and its magnitude grows slowly up to a film thickness of 6 μm, after which it varies little. These observations show that 6 μm of PET is virtually opaque at 1730 cm^{-1}, and that the amount of signal generated deeper than 2.5 μm is too small to affect the phase of the total signal (within experimental error). The polycarbonate band magnitude monotonically decreases as the film thickness increases, because the thermal wave generated in the polycarbonate has increasingly far to diffuse. By contrast, the phase for the polycarbonate band does not monotonically increase with thickness as Eq. 7 requires. The phase increases to a maximum of 183° (3° after wrapping around to the start of the phase scale) for the 12-μm sample; then it actually decreases for the 23-μm sample. A plot of the depths of the polycarbonate substrates against the observed phases of the polycarbon-

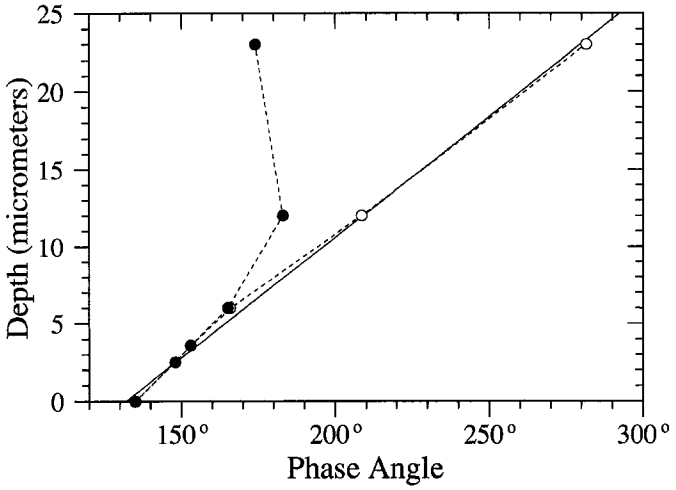

FIG. 7. Relation between depth of the polycarbonate substrate (thickness of PET layer) and the phase of the 1778-cm^{-1} polycarbonate peak; (•) observed phases from Fig. 6B; (○) phases corrected by using Eq. 9; and (———) theoretical prediction from Eq. 7.

ate band is shown as the solid circles in Fig. 7. The solid line in the figure is the theoretical prediction from Eq. 7, based on a thermal diffusivity of 0.0010 cm^2/s from data in Ref. 15 (giving a thermal diffusion length of 8.9 μm at 400 Hz) and using an abscissa intercept of 132° (chosen to minimize the error of the corrected phases discussed below). The figure shows that the bare through 6-μm samples obey Eq. 7, but both the 12- and 23-μm samples deviate substantially. This deviation is caused by band overlap; the thicker PET films are not transparent at 1778 cm^{-1} as Eq. 7 requires. The wing of the 1730-cm^{-1} PET band is sufficiently strong at 1778 cm^{-1} to shift the observed phase toward that of the PET band. We can correct the observed phase and magnitude for the effects of the band overlap by recognizing that the total observed signal is the vector sum of the polycarbonate and PET contributions. Consider a total signal, T, having magnitude M_T and phase θ_T, that is the sum of polycarbonate and PET vectors having magnitudes M_{PC} and M_{PET} and phases θ_{PC} and θ_{PET}, respectively. M_{PC} and θ_{PC} can be found from T and the PET vector by standard geometry:

$$M_{PC} = [M_T^2 + M_{PET}^2 - 2M_T M_{PET}\cos(\theta_T - \theta_{PET})]^{1/2} \quad (8)$$

$$\theta_{PC} = \theta_T + \cos^{-1}\left(\frac{M_T^2 + M_{PC}^2 - M_{PET}^2}{2M_T M_{PC}}\right). \quad (9)$$

The PET contribution at 1778 cm^{-1} must be measured separately from the rest of the sample in order to perform the geometric subtraction given by Eqs. 8 and 9. Fortunately, the observed phase diverges substantially from the Eq. 7 prediction only when the PET layer is thicker than a thermal diffusion length, so the phase and magnitude of the contribution from the PET film should not depend much on the film thickness. A thick sheet of PET therefore should make a good sample for determining the PET contribution. Its front-surface photoacoustic signal should match those of the films, and like the films attached to thick polycarbonate substrates, it should have no rear-surface signal. Figure 8 shows the phase and power spectra for the samples with 12- and 23-μm PET layers and for a 0.74-mm-thick sheet of PET, with the power spectra

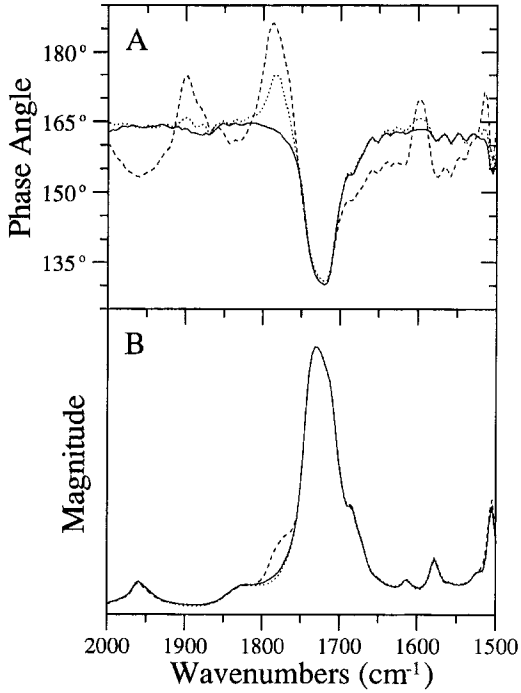

FIG. 8. (**A**) Phase spectra and (**B**) power spectra of samples consisting of (———) thick PET sheet and of a polycarbonate substrate covered by (·····) a 23-μm PET film and by (- - -) a 12-μm PET film. The power spectra have been scaled to match at the 1730-cm^{-1} peak.

scaled to match at the 1730-cm^{-1} peak. This scaling to match up the peak of the overlapping band should be done before determining the magnitudes for Eqs. 8 and 9. The power spectrum for the 12-μm sample has a definite shoulder from the 1778-cm^{-1} polycarbonate band, but the 23-μm spectrum does not. In fact, the 23-μm spectrum is slightly *weaker* than the pure-PET spectrum at that wavenumber. This counterintuitive result occurs whenever the phase of the substrate contribution lags behind (is greater than) that of the complete sample by more than 90°. The numerator in Eq. 9 must then be negative, so $M_{PET} > M_T$. The phase spectra are much more sensitive to the presence of the substrate than the power spectra. Not only is the 1778-cm^{-1} band clearly present in both the 12- and 23-μm sample phase spectra, but the positive-going features at 1898 and 1599 cm^{-1} indicate other known polycarbonate bands, even though the power spectra do not show them. (The phase peak at 1516 cm^{-1} is the shoulder of another polycarbonate peak hidden behind the 1504-cm^{-1} peak of PET.) The open circles in Fig. 7 are the phases of the polycarbonate substrate after correction with the use of data from Fig. 8 in Eqs. 8 and 9. The corrected data fit the theoretical line well; the rms error of the corrected phases is 0.41 μm (or 2.6°).

CONCLUSION

Phase-modulation FT-IR photoacoustic spectroscopy has a variety of uses in depth profiling layered samples. We have demonstrated that it can determine quantitatively the thicknesses of layers, even in cases of band overlap and at depths greater than twice the thermal diffusion length. We have discussed various ways the phase-modulation data may be represented and described how these

representations may be derived from a single pair of orthogonal interferograms.

ACKNOWLEDGMENTS

The authors wish to thank the Digilab Division of Bio-Rad for loan of a Bio-Rad FTS 60A FT-IR spectrometer used for some of the work reported here, and for technical support. The authors thank Dr. Stanley Bajic for critical readings of the manuscript. Ames Laboratory is operated for the U.S. Department of Energy by Iowa State University under Contract No. W-7405-ENG-82. This work was supported in part by the U.S. Department of Energy, Office of Science and Technology.

1. J. C. Donini and K. H. Michaelian, Infrared Phys. **24,** 157 (1984).
2. M. W. Urban and J. L. Koenig, Appl. Spectrosc. **40,** 994 (1986).
3. C. Q. Yang, R. R. Bresee, and W. G. Fateley, Appl. Spectrosc. **41,** 889 (1987).
4. A. Rosencwaig and A. Gersho, J. Appl. Phys. **47,** 64 (1976).
5. M. J. Adams and G. F. Kirkbright, Analyst **102,** 281 (1977).
6. R. A. Palmer, J. L. Chao, R. M. Dittmar, V. G. Gregoriou, and S. E. Plunkett, Appl. Spectrosc. **47,** 1297 (1993).
7. R. A. Palmer, C. J. Manning, J. L. Chao, I. Noda, A. E. Dowrey, and C. Marcott, Appl. Spectrosc. **45,** 12 (1991).
8. V. G. Gregoriou, M. Daun, M. W. Schauer, J. L. Chao, and R. A. Palmer, Appl. Spectrosc. **47,** 1311 (1993).
9. R. M. Dittmar, J. L. Chao, and R. A. Palmer, Appl. Spectrosc. **45,** 1104 (1991).
10. R. A. Palmer and R. M. Dittmar, Thin Solid Films **223,** 31 (1993).
11. M. G. Sowa and H. H. Mantsch, Appl. Spectrosc. **48,** 316 (1994).
12. L. E. Jurdana, K. P. Ghiggino, I. H. Leaver, and P. Cole-Clarke, Appl. Spectrosc. **49,** 361 (1995).
13. E. Y. Jiang, R. A. Palmer, and J. L. Chao, J. Appl. Phys. **78,** 460 (1995).
14. Y. C. Teng and B. S. H. Royce, J. Opt. Soc. Am. **70,** 557 (1980).
15. D. R. Anderson and R. U. Acton, "Thermal Properties", in *Encyclopedia of Polymer Science and Technology,* H. F. Mark, N. G. Gaylord, and N. M. Bikales, Eds. (Wiley–Interscience, New York, 1970), Vol. 13, pp. 780–781, Table 4.